Bus Participation Factor Analysis for Harmonic Instability in Power Electronics Based Power Systems

Ebrahimzadeh, Esmaeil; Blaabjerg, Frede; Wang, Xiongfei; Bak, Claus Leth

Published in:
I E E E Transactions on Power Electronics

DOI (link to publication from Publisher):
10.1109/TPEL.2018.2803846

Publication date:
2018

Document Version
Publisher's PDF, also known as Version of record

Bus Participation Factor Analysis for Harmonic Instability in Power Electronics Based Power Systems

Esmaeil Ebrahimzadeh, *Student Member, IEEE*, Frede Blaabjerg, *Fellow, IEEE*, Xiongfei Wang, *Senior Member, IEEE*, and Claus Leth Bak, *Senior Member, IEEE*

***Abstract*—Compared with the conventional power systems, large-scale power electronics based power systems present a more complex situation, where harmonic instability may be induced by the mutual interactions between the inner control loops of the converters. This paper presents an approach to locate which power converters and buses are more sensitive and have a significant contribution to the harmonic instability. In the approach, a power electronics based system is introduced as a multi-input multi-output (MIMO) dynamic system by means of a dynamic admittance matrix. Bus participation factors (PFs) are calculated by the oscillatory mode sensitivity analysis versus the elements of the MIMO transfer function matrix. The PF analysis detects which power electronic converters or buses have a higher participation in harmonic instability excitation than others or at which buses such instability problems have a higher impact. In order to confirm the effectiveness of the presented approach, time-domain simulation results are provided for a 400-MW wind farm in PSCAD software environment.**

***Index Terms*—Harmonic instability, power electronics based systems, participation factor (PF) analysis, sensitivity analysis.**

I. Introduction

THE integration of the power electronic converters into the electric power system has been increased over the last decades because of the extensive usage in different industrial and commercial applications such as renewable energy sources, electric railway systems, variable-speed drivers, HVDC, and flexible alternating current transmission system (FACTS) [1], [2]. Besides the advantages, including full controllability and improved efficiency, high penetration of power electronics based power systems is challenging the stable operation of the power delivery system [3]–[5]. Some stability studies in power electronics based systems have focused on low-frequency oscillations, driven by the outer controllers of power converters [6], [7] and phase-locked loops [8]–[10]. Apart from the low-frequency oscillations, the mutual interactions between the fast inner control loops of the grid-connected converters may lead to high-frequency oscillations, which can be called harmonic instability [9]. Most research works about harmonic instability discuss how to predict a system is either stable or unstable. However, it has not been paid much attention to identify which power converters have more influence on the harmonic instability or which buses are affected more by the harmonic instability than others. A general approach for analyzing such stability is based on the state-space model, where the stability can be assessed by eigenvalue analysis of the state-space matrix [12]–[21]. In state-space modeling, the participation factor (PF) contribution of each state variable to the system stability can be calculated based on the eigenvectors of the state matrix [15]–[21]. The state-space analysis has been applied in some systems such as inverter-based microgrid [14], active-rectifier-based microgrid [15], current source inverters [12], parallel-connected inverters [13], [18], and wind farms [19], [21]. However, in a large-scale power system with a high penetration of power electronic converters, there would be a lot of state variables, coming from the detailed models of power converter dynamics, loads, cables, transformers, etc., required. Therefore, the formulation of the state matrices may become complicated in such large systems [21]–[23]. Apart from the state-space analysis, the impedance-based analysis approach is another powerful tool to predict the harmonic instability by calculating the ratio of the converter output impedance to the grid equivalent impedance at point of connection (PoC) of the converter [24]–[27]. The impedance-based approach has been applied in several applications, e.g., parallel *LCL*-filtered grid-connected converters [28], and voltage-controlled and current-controlled inverters with *LC*- and *LCL* filters [11]. However, the impedance-based analysis is not able to locate which bus and which converter in a large power electronics based power system has the most contribution to harmonic instability [29], [30].

In contrast to the previous research works [15]–[21], where PF analysis for the system stability is presented based on the state-space modeling, this paper presents a new PF analysis for the system stability based on a multi-input multi-output (MIMO) transfer function matrix. A large-scale power electronics based system is modeled as a MIMO transfer function matrix by means of the nodal admittance matrix of the system. Since the presented approach is based on the nodal admittance matrix of the power system, it is easy to apply for a large power electronics based system. PFs and sensitivities of different buses and power electronic converters to the harmonic instability are calculated by

Manuscript received August 11, 2017; revised December 19, 2017; accepted February 4, 2018. Date of publication March 9, 2018; date of current version September 28, 2018. This work was supported by the European Research Council under the European Union's Seventh Framework Program (FP/2007-2013)/ERC Grant Agreement no. [321149-Harmony]. Recommended for publication by Associate Editor Jesus A Oliver. *(Corresponding author: Esmaeil Ebrahimzadeh.)*

The authors are with the Department of Energy Technology, Aalborg University, Aalborg DK-9220, Denmark (e-mail: ebb@et.aau.dk; fbl@et.aau.dk; xwa@et.aau.dk; Clb@et.aau.dk).

Color versions of one or more of the figures in this paper are available online at http://ieeexplore.ieee.org.

Digital Object Identifier 10.1109/TPEL.2018.2803846

means of mode analysis of the introduced MIMO system. Since PFs are the product of the controllability and the observability of harmonic instability at the system buses, a power converter and a bus with a larger PF are more sensitive and have more contribution to the harmonic instability. Therefore, the advantages of the proposed PF analysis can be summarized as follows.

1) It is a systematic approach and easy to apply to large power electronics based power systems like large wind farms, where a large number of power converters, transformers, long cables, and filters are located.
2) By changing a component of the system, only one admittance of the system is affected. Therefore, the effects of new changes on system stability can be easily analyzed.
3) The detailed information of each component of the system is not needed.
4) When a component model is black-box, its equivalent admittance can be obtained by experiment (if the component has been built) or by numerical simulations (if the component has been designed but has not been built yet).
5) It is simple to identify directly which component of the system has more contribution to instability and which component is the main source of instability.

Other contributions of this paper are as follows.

1) Most of the research works about stability of power electronic systems discuss small-scale systems, where individual or small groups of power electronic converters are considered [18], [28]. However, it has been paid less attention to large-scale power electronic systems. On the other hand, about large-scale power electronic system stability, it has not been paid much attention to the effects of the dynamics and the time-delay of the digital control system and pulsewidth modulation (PWM) [19], [21]. However, a large volume of the literature about the individual grid-connected converters has shown that the time-delay of the digital control system and PWM have a significant effect on the stability of the system [31]–[33]. Therefore, this paper attempts to fill in this gap, i.e., PF analysis of a large-scale power electronic system with considering the effects of the time delay of the digital control system and PWM.
2) The effects of connection/disconnection of the power converters with different PFs are analyzed. Therefore, PFs can locate the main source of harmonic instability and the most efficient location for damping and reducing the harmonic instability problems.
3) The grid disturbance amplification by the resonance modes with very low damping is analyzed. The PF analysis shows that which bus amplifies the grid harmonic background more.
4) The effect of the cable lengths on the system stability is analyzed.
5) The electrical oscillations during faults and transients are predicted by the PF analysis.

In Section II, a grid-connected converter is modeled as a current source with a parallel active admittance. In Section III, a large power electronics based power system is introduced as a MIMO system using the admittance matrix of the whole system. The mode analysis is presented in Section IV, where PFs of the system buses for the oscillatory modes are calculated. In addition, the damping and the frequency of oscillations, and the most and least influencing bus for each mode are obtained. In Section V, the mode and PF analysis results are validated by nonlinear time-domain simulation for a 400-MW wind farm as a case study, where the effectiveness of the proposed method is demonstrated. In Section VI, the conclusion is presented.

II. Grid-Connected Converter Model

Fig. 1(a) shows a block diagram of a three-phase grid-connected voltage source converter. As the system is assumed to be a three-phase balanced system, the converter can be modeled by its single-phase equivalent circuit, as shown in Fig. 1(b), where $G_{\text{cont}-k}$ is the current controller, and $G_{\text{delay}-k}$ is the delay of the digital control and SPWM. As the output of the current controller is normalized to the dc-link voltage, the gain of the system is equal to 1 in Fig. 1(b). Fig. 1(c) depicts the block diagram of the current closed-loop control, where the PoC voltage $(V_{\text{PoC}-k})$ and the current reference $(I_{\text{ref}-k})$ are the inputs and the grid current (I_{g-k}) is the output. From Fig. 1(c), the grid current can be obtained as follows:

$$I_{g-k} = G_{c-k} I_{\text{ref}-k} - Y_{c-k} V_{\text{PoC}-k} \tag{1}$$

where G_{c-k} and Y_{c-k} are

$$G_{c-k} = \frac{T_{c-k}}{1 + T_{c-k}}, \quad Y_{c-k} = \frac{Y_{Lf-k}}{1 + T_{c-k}}. \tag{2}$$

T_{c-k} and Y_{Lf-k} are

$$T_{c-k} = G_{\text{cont}-k} G_{\text{delay}-k} Y_{Lf-k}, \quad Y_{Lf-k} = \frac{1}{sL_{f-k}}. \tag{3}$$

Based on (1), a current-controlled grid-connected converter can be modeled as a Norton equivalent, i.e., a current source with a parallel active admittance, as shown in Fig. 1(d). This paper focuses on the harmonic instability above the fundamental frequency. Therefore, the outer power controllers and grid synchronization loops are neglected because they are too slow to have the influence on the high-frequency oscillations.

In this paper, $G_{\text{cont}-k}$ is considered with a proportional plus resonant current controller and $G_{\text{delay}-k}$ is modeled by Pade approximation, i.e.,

$$\begin{aligned} G_{\text{cont}-k} &= K_{p-k} + \frac{K_{i-k} s}{s^2 + \omega_f^2}, \quad G_{\text{delay}-k}(s) = e^{-1.5 T_{s,k} s} \\ &\approx \frac{1 - \frac{1.5T_{s-k}}{2} s + \frac{(1.5T_{s-k})^2}{10} s^2}{1 + \frac{1.5T_{s-k}}{2} s + \frac{(1.5T_{s-k})^2}{10} s^2} \end{aligned} \tag{4}$$

where ω_f and T_{s-k} are the fundamental frequency of the grid and the sampling period of the digital control, respectively. As the SPWM with the double update has been considered, the sampling period (T_{s-k}) is equal to $\frac{0.5}{f_{\text{sw}}}$, where f_{sw} is the switching frequency [31]–[33].

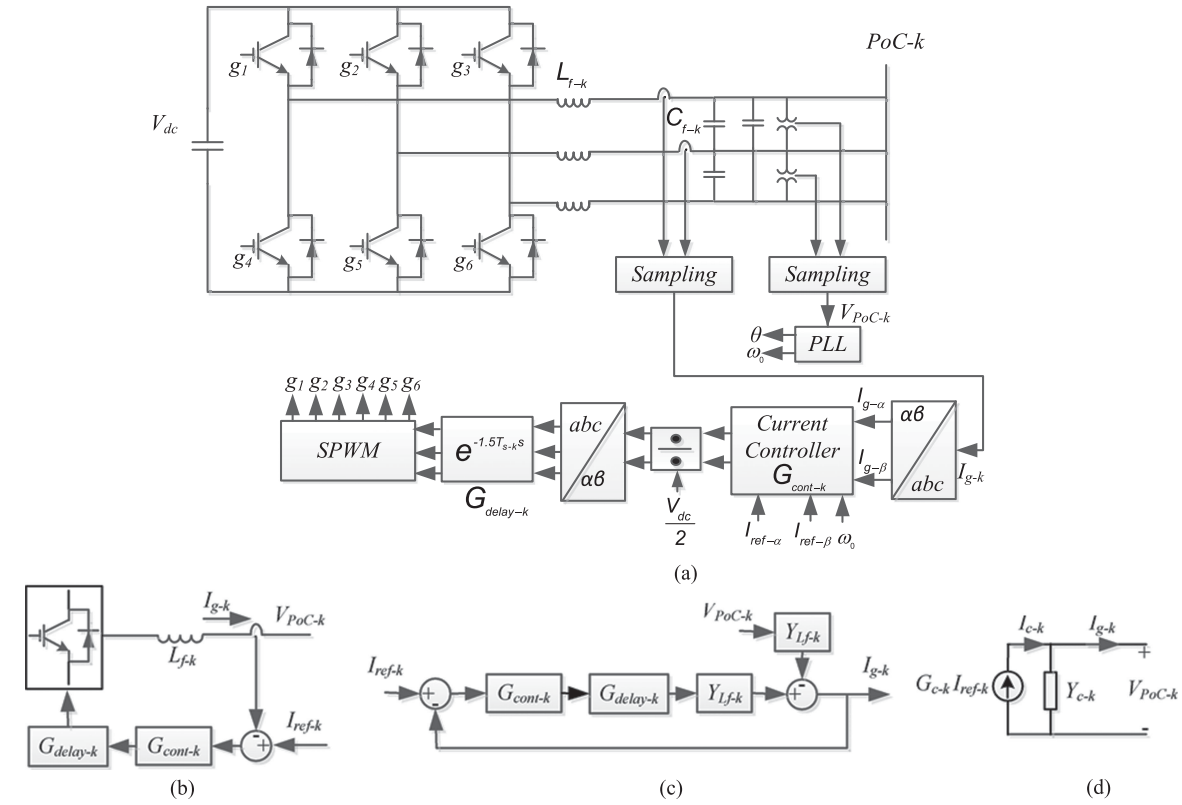

Fig. 1. Grid-connected converter along with the current control system. (a) Three-phase grid-connected voltage source converter. (b) Single-phase equivalent circuit of the converter. (c) Block diagram of closed-loop control of grid current. (d) Norton equivalent model of the converter.

III. Power Electronics Based System as a Multi-Input Multi-Output (MIMO) Transfer Function Matrix

By applying the Norton equivalent theorem for every passive element and active element (grid-connected converters) in the *s*-domain, the current–voltage relationships can be written by using the nodal admittance matrix of the power system as (5) as shown at the bottom of this page, where it is assumed that bus-1 is connected to the main electrical grid and bus-2 to bus $n+1$ are connected to the power converters. Bus $n+2$ to bus m are other buses to which any power converters or grid are not connected. $Y_{c-k}\,(k=1,2,\ldots,n), Y_{ii}, Y_{ij}(s)\,(i,j=1,2,\ldots,m, \text{and}\, i\neq j)$ are the active admittance of the kth power converter, the connected admittance to the ith bus, and the admittance between ith bus and jth bus, respectively. Equation (5) is actually a MIMO transfer function matrix, where the outputs are the bus voltages and the inputs are the injected currents, i.e.,

$$\mathbf{V}(\mathbf{s}) = \mathbf{G}(\mathbf{s})^{-1}\mathbf{I}(\mathbf{s}). \tag{6}$$

The poles of the introduced MIMO transfer function are the oscillatory modes of the power system, which can be obtained by solving the following equation:

$$\det\left[\mathbf{G}(\mathbf{s})\right] = 0$$
$$\Rightarrow p_1 = \alpha_1 + j\beta_1, p_2 = \alpha_2 + j\beta_2, \ldots, p_q = \alpha_q + j\beta_q \tag{7}$$

where the oscillation frequency (f_i) and the damping ratio (ζ_i) of the oscillations can also be obtained by

$$f_i = \frac{\beta_i}{2\pi} \quad \zeta_i = \frac{-\alpha_i}{\sqrt{\alpha_i^2+\beta_i^2}}. \tag{8}$$

$$\begin{bmatrix} I_g \\ I_{c-1} \\ I_{c-2} \\ \vdots \\ I_{c-n} \\ 0 \\ \vdots \\ 0 \end{bmatrix} = \begin{bmatrix} Y_{11} & -Y_{12} & -Y_{13} & \cdots & -Y_{1(n+1)} & -Y_{1(n+2)} & \cdots & -Y_{1m} \\ -Y_{21} & Y_{22}+Y_{c-1} & -Y_{23} & \cdots & -Y_{2(n+1)} & -Y_{2(n+2)} & \cdots & -Y_{2m} \\ -Y_{31} & -Y_{32} & Y_{33}+Y_{c-2} & \cdots & -Y_{3(n+1)} & -Y_{3(n+2)} & \cdots & -Y_{3m} \\ \vdots & \vdots & \vdots & \vdots & \vdots & \vdots & \vdots & \vdots \\ -Y_{(n+1)1} & -Y_{(n+1)2} & -Y_{(n+1)3} & \cdots & Y_{(n+1)(n+1)}+Y_{c-n} & Y_{(n+1)(n+2)} & \cdots & -Y_{(n+1)m} \\ -Y_{(n+2)1} & -Y_{(n+2)2} & -Y_{(n+2)3} & \cdots & -Y_{(n+2)(n+1)} & Y_{(n+2)(n+2)} & \cdots & -Y_{(n+2)m} \\ \vdots & \vdots & \vdots & \vdots & \vdots & \vdots & \vdots & \vdots \\ -Y_{m1} & -Y_{m2} & -Y_{m3} & \cdots & -Y_{mn} & -Y_{m(n+2)} & \cdots & Y_{mm} \end{bmatrix} \begin{bmatrix} V_1 \\ V_2 \\ V_3 \\ \vdots \\ V_n \\ V_{(n+1)} \\ \vdots \\ V_m \end{bmatrix} \tag{5}$$

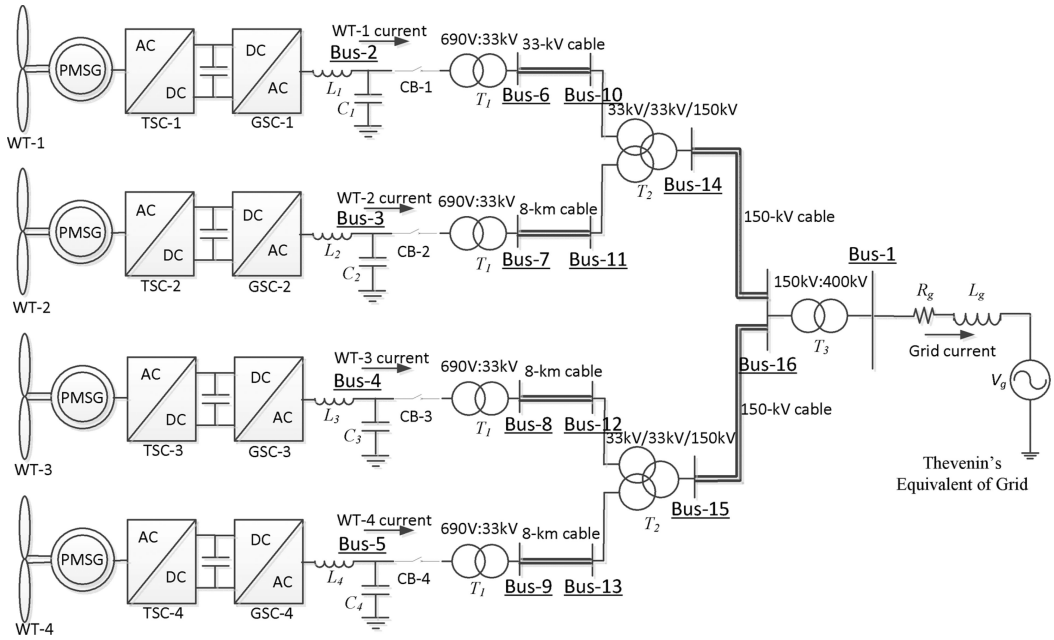

Fig. 2. 400-MW wind farm studied in this paper for the proposed participation factor analysis.

TABLE I
PARAMETERS OF THE 400-MW WIND FARM

Parameter		Value
Transformer T_1	Leakage inductance	1.378 μH
33-kV cable (Cable $_{33-\mathrm{kV}}$)	Shunt capacitance	3.24 μF
	Series inductance	0.436 mH
	Series resistance	0.0537 Ω
Transformer T_2	Leakage inductance	1.891 mH
150-kV cable (Cable $_{150-\mathrm{kV}}$)	Shunt capacitance	0.26 μF/km
	Series inductance	0.5 mH/km
	Series resistance	0.0574 Ω/km
Transformer T_3	Leakage inductance	22.788 mH
Grid	X/R ratio	20
	SCR	100

TABLE II
PARAMETERS OF GRID-SIDE CONVERTERS (GSCS) FOR WT-1 TO WT-4

Parameter			Value
GSC-1	Filter	*inductor (L_1)*	0.9 µH
		Capacitor (C_1)	84 mF
	Controller	*Switching frequency ($f_{sw,1}$)*	4 kHz
		Bandwidth	530 Hz
		$K_{p,1}$	1.6e-3
		$K_{i,1}$	541e-3
GSC -2	Filter	*Inductor (L_2)*	1.78 µH
		Capacitor (C_2)	161 mF
	Controller	*Switching frequency ($f_{sw,2}$)*	2.5 kHz
		Bandwidth	425 Hz
		$K_{p,2}$	2.2e-3
		$K_{i,2}$	1082e-3
GSC -3	Filter	*Inductor (L_3)*	0.9 µH
		Capacitor (C_3)	202 mF
	Controller	*Switching frequency ($f_{sw,3}$)*	3.5 kHz
		Bandwidth	465 Hz
		$K_{p,3}$	1.4e-3
		$K_{i,3}$	433e-3
GSC-4	Filter	*Inductor (L_4)*	0.13 µH
		Capacitor (C_4)	367 mF
	Controller	*Switching frequency ($f_{sw,4}$)*	4 kHz
		Bandwidth	525 Hz
		$K_{p,4}$	0.12e-3
		$K_{i,4}$	450e-3

The poles of the MIMO transfer function matrix basically are the poles of its elements, i.e.,

$$G_{ij}(s) = \frac{P(s)}{(s-p_1)(s-p_2)\cdots(s-p_q)} = \frac{A_1}{(s-p_1)} + \frac{A_2}{(s-p_2)} + \cdots + \frac{A_q}{(s-p_q)}. \quad (9)$$

The inverse Laplace transform of $G_{ij}(s)$ is

$$G_{ij}(t) = A_1 e^{p_1 t} + A_2 e^{p_2 t} + \cdots + A_q e^{p_q t} = A_1 e^{\alpha_1 t} e^{j\beta_1 t} + A_2 e^{\alpha_2 t} e^{j\beta_2 t} + \cdots + A_q e^{\alpha_q t} e^{j\beta_q t}. \quad (10)$$

Therefore, the poles of $G_{ij}(s)$ in the s-domain show the oscillations of $G_{ij}(t)$ in the time domain. The imaginary parts of the poles show the oscillation frequencies and the real parts show the damping of the oscillations. If α_q (one of the real parts) is positive, the term $A_q e^{\alpha_q t} e^{j\beta_q t}$ is an increasing exponential and

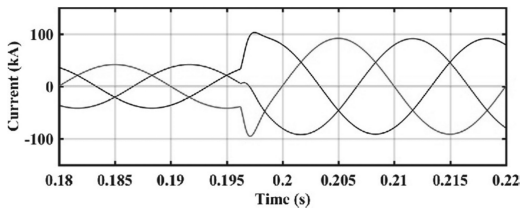

Fig. 3. Step response of GSC-1 for a strong grid.

TABLE III
FREQUENCY, DAMPING, PARTICIPATION FACTOR, AND INFLUENCING BUSES FOR THE OSCILLATORY MODES OF THE WIND FARM ($L_{\text{CABLE}} = 10$ KM)

Mode i	Real part α_i	Frequency f_i	Damping ζ_i	The largest participation factor (PF_i)	The smallest participation factor (PF_i)	The most influencing bus	The least influencing bus
p_1	–33.5928	67.07399	0.079458	0.197011	0.001399	4	1
p_2	–104.447	70.33675	0.230002	0.550534	0.000291	2	1
p_3	–33.6531	73.03792	0.073136	0.670614	0.00217	5	1
p_4	–133.93	85.53932	0.241796	0.720086	0.000429	3	1
p_5	–379.337	428.1876	0.139617	0.393558	3.25E – 05	3	5
p_6	–629.545	492.4904	0.199362	0.667492	8.05E–05	4	5
p_7	–127.862	586.1375	0.034698	0.156834	0.00054	14	5
p_8	–489.454	784.0175	0.098872	0.7446	0.00029	2	3
p_9	20.58653	839.9291	–0.0039	0.737738	0.000128	5	4
p_{10}	–43.8898	1888.711	0.003698	0.116899	4.82E–08	13	1
p_{11}	–15957.6	2429.353	0.722635	1.02945	0	3	5
p_{12}	–19.6983	2463.564	0.001273	0.136212	1.10E – 05	7	5
p_{13}	–0.23499	2570.186	1.46E–05	0.262655	4.39E–10	8	14
p_{14}	0.006365	2578.026	3.93E–07	0.264195	4.03E–09	6	5
p_{15}	–8.90394	2810.927	0.000504	0.136762	7.02E–08	6	1
p_{16}	–35.659	3048.901	0.001861	0.126374	3.97E–06	9	5
p_{17}	–22171.4	3321.399	0.728172	1.015231	0	4	3
p_{18}	–23068.1	3350.696	0.738632	1.013194	0	5	3
p_{19}	–25313.3	3797.759	0.727659	1.009835	0	2	5
p_{20}	–56.3225	8853.221	0.001013	0.266982	0	13	14
p_{21}	–56.3185	8853.384	0.001012	0.27569	0	11	5
p_{22}	–56.2355	8856.541	0.001011	0.267144	3.69E–10	12	3
p_{23}	–56.2315	8856.707	0.00101	0.275829	7.45E–11	10	5

TABLE IV
PARTICIPATION FACTORS OF BUSES 2–5 FOR THE UNSTABLE MODE

Bus number	PF for the unstable mode ($P_9 = 20.587 \pm 5277.43i$)
Bus-2 (GSC-1)	0.1095e – 1
Bus-3 (GSC-2)	0.346e – 3
Bus-4 (GSC-3)	0.128e – 3
Bus-5 (GSC-4)	0.737738

the system is unstable. If α_q is negative, $A_q e^{\alpha_q t} e^{j\beta_q t}$ is a decaying exponential function with a final value of zero. Therefore, for a system to be stable, all real parts of the poles ($p_1, p_2, \ldots,$ and p_q) must be in the left half of the s-plane.

IV. PROPOSED BUS PARTICIPATION FACTOR ANALYSIS

By substituting the modes (p_q) for s in the transfer function matrix of $\mathbf{G}(\mathbf{s})$, $\mathbf{G}(p_q)$ can be numerically obtained. Based on the theory of the eigenvalue decomposition [34]–[37], the matrix $\mathbf{G}(p_q)$ can be decomposed into three matrixes as

$$\mathbf{G}(p_q) = \mathbf{R}\mathbf{\Lambda}\mathbf{L} = \mathbf{R}\begin{bmatrix} \lambda_1 & 0 & 0 & 0 \\ 0 & \lambda_2 & 0 & 0 \\ 0 & 0 & \cdots & 0 \\ 0 & 0 & 0 & \lambda_m \end{bmatrix}\mathbf{L} \tag{11}$$

where $\mathbf{\Lambda}$ is a diagonal matrix whose diagonal elements are the eigenvalues of $\mathbf{G}(p_q)$ $(\lambda_1, \lambda_2, \ldots, \lambda_m)$. $\mathbf{R}$ is a matrix whose columns are the corresponding right eigenvectors, i.e.,

$$\mathbf{G}(p_q)\mathbf{R} = \mathbf{R}\mathbf{\Lambda}. \tag{12}$$

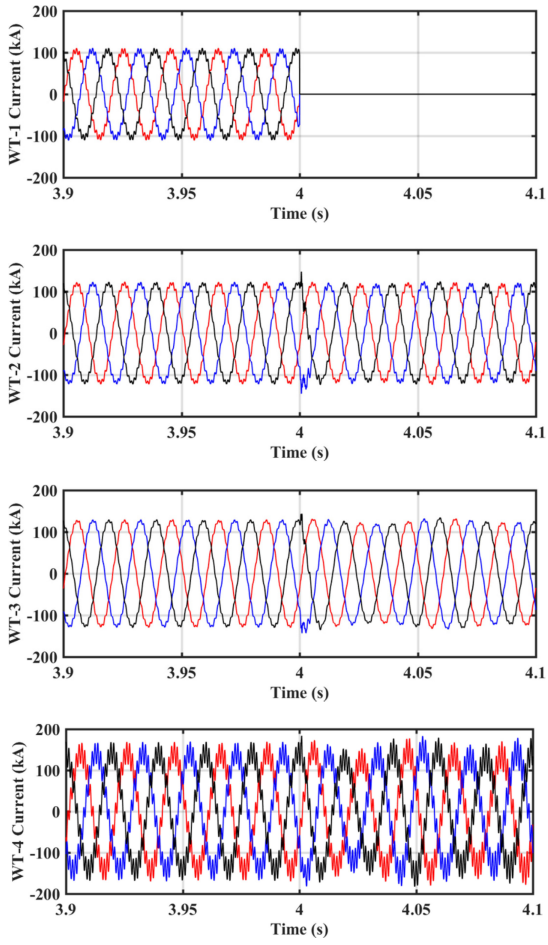

Fig. 4. Currents injected by WT-1, WT-2, WT-3, and WT-4, where WT-1 is disconnected at $t = 4$ s.

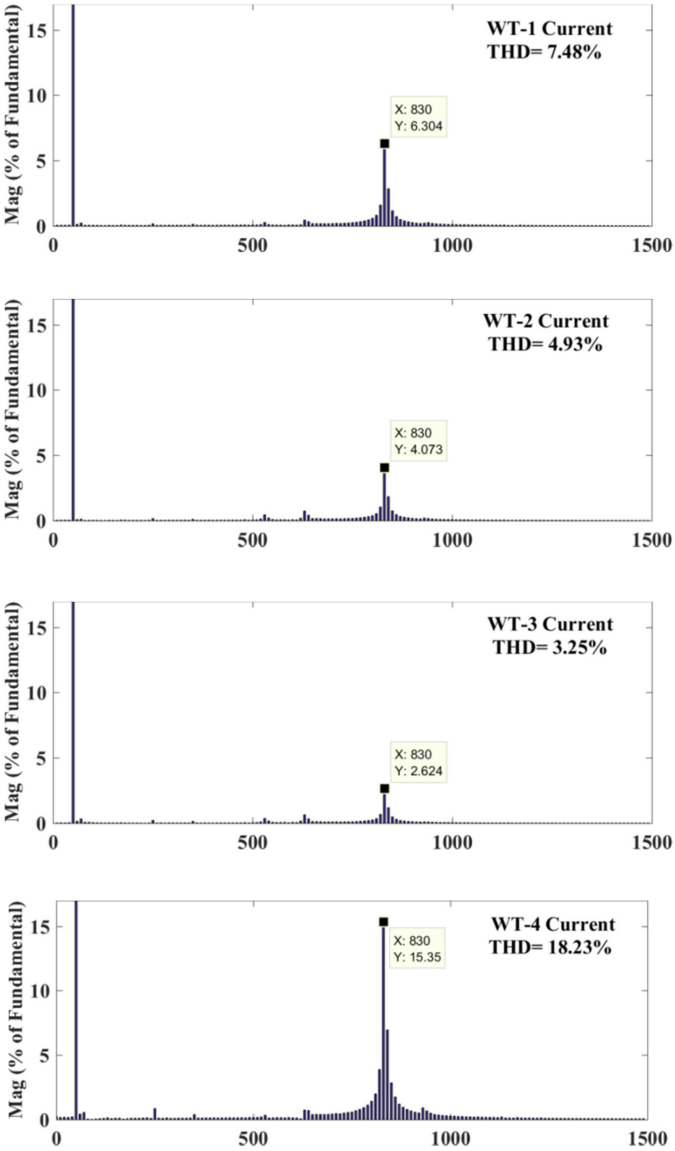

Fig. 5. FFT analysis of the waveforms shown in Fig. 4 before $t = 4$ s, when all WTs are connected.

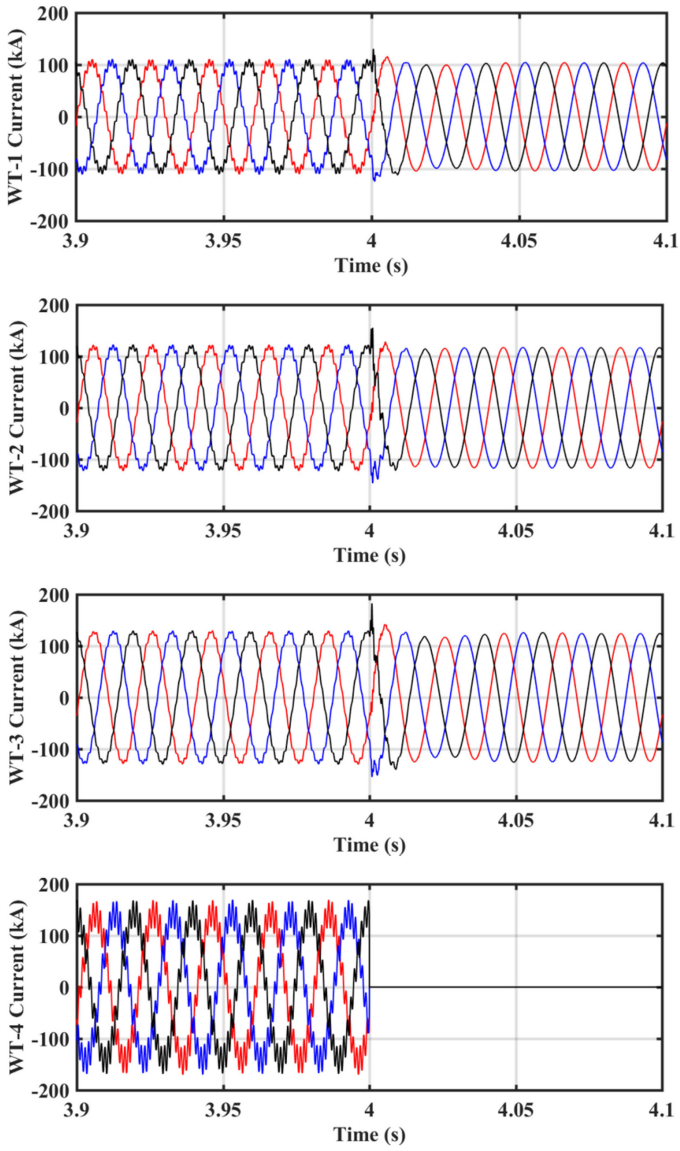

Fig. 6. Currents injected by WT-1, WT-2, WT-3, and WT-4, where WT-4 is disconnected at $t = 4$ s.

$\mathbf{L}$ is a matrix whose rows are transposed left eigenvectors, i.e.,

$$\mathbf{L}\mathbf{G}(p_q) = \mathbf{\Lambda}\mathbf{L}. \tag{13}$$

The following equation can be obtained from (12) and (13):

$$\mathbf{L} = \mathbf{R}^{-1}. \tag{14}$$

Using (11) and (14), the inverse of $\mathbf{G}(p_q)$ can be derived from

$$\mathbf{G}^{-1}(p_q) = \mathbf{R}\mathbf{\Lambda}^{-1}\mathbf{L} = \mathbf{R}\begin{bmatrix} 1/\lambda_1 & 0 & 0 & 0 \\ 0 & 1/\lambda_2 & 0 & 0 \\ 0 & 0 & \cdots & 0 \\ 0 & 0 & 0 & 1/\lambda_m \end{bmatrix}\mathbf{L}. \tag{15}$$

Since p_q is a pole of the $\mathbf{G}^{-1}(\mathbf{s})$, one of the eigenvalues of $\mathbf{G}(p_q)$ ($\lambda_1, \lambda_2, \ldots,$ or λ_m) should ideally be equal to zero. However, it is close to but not exactly zero because of the round-off errors of floating-point computations. The mentioned eigenvalue, i.e., the smallest eigenvalue is called the critical eigenvalue (λ_c) and its right and left eigenvectors are called the critical right and left eigenvectors ($\boldsymbol{r}_c$ and $\boldsymbol{l}_c$). If the ith eigenvalue is λ_c, the ith column of the matrix $\mathbf{R}$ is $\boldsymbol{r}_c$ and the ith row of the matrix $\mathbf{L}$ is $\boldsymbol{l}_c$. The sensitivity of the critical eigenvalue with respect to the $\mathbf{G}(p_q)$ elements can then be calculated by the multiplication of the ith right eigenvector and the transposed ith left eigenvector:

$$\mathbf{S}_{\lambda c} = \frac{\partial \lambda_c}{\partial\left[\mathbf{G}(p_q)\right]} = \mathbf{r}_c\mathbf{l}_c. \tag{16}$$

TABLE V
FREQUENCY, DAMPING, PARTICIPATION FACTOR, AND INFLUENCING BUSES FOR THE OSCILLATORY MODES OF THE WIND FARM ($L_{\text{CABLE}} = 5$ KM)

Mode i	Real part α_i	Frequency f_i	Damping ζ_i	The largest participation factor (PF_i)	The smallest participation factor (PF_i)	The most influencing bus	The least influencing bus
p_1	–37.322	67.67661	0.087434	0.215021	0.001483	4	1
p_2	–107.229	70.55648	0.235098	0.575217	0.000299	2	1
p_3	–30.7038	72.82643	0.06695	0.581145	0.001978	5	1
p_4	–134.65	85.9258	0.241991	0.720008	0.000444	3	1
p_5	–373.717	439.6441	0.134067	0.54612	1.89E – 05	3	5
p_6	–672.616	495.9811	0.210977	0.592752	4.10E – 05	4	5
p_7	–417.47	732.4515	0.090341	0.339319	0.001657	2	5
p_8	–99.631	818.1231	0.019378	0.165125	0.002907	5	4
p_9	–33.0973	862.8075	0.006105	0.167917	0.002285	16	4
p_{10}	–15957.6	2429.353	0.722635	1.029948	4.25E – 12	3	5
p_{11}	–8.17791	2438.652	0.000534	0.134898	9.84E – 08	9	1
p_{12}	–0.23348	2570.18	1.45E – 05	0.26203	1.66E – 09	8	14
p_{13}	–0.006739	2577.957	4.16E – 07	0.265142	1.70E – 08	7	5
p_{14}	–1.98489	2666.263	0.000118	0.147683	7.26E – 06	6	5
p_{15}	–22171.4	3321.399	0.728172	1.015238	0	4	3
p_{16}	–23068.1	3350.696	0.738632	1.0132	0	5	3
p_{17}	–25313.3	3797.759	0.727659	1.009821	0	2	5
p_{18}	–47.18	4257.028	0.001764	0.330987	2.36E – 11	15	1
p_{19}	–54.7767	5707.849	0.001527	0.310775	4.72E – 08	14	5
p_{20}	–56.3225	8853.222	0.001013	0.263699	0	13	14
p_{21}	–56.3185	8853.385	0.001012	0.267184	0	11	5
p_{22}	–56.1097	8861.298	0.001008	0.170296	1.05E – 08	12	1
p_{23}	–56.0949	8861.868	0.001007	0.17244	3.47E – 08	10	5

TABLE VI
PARTICIPATION FACTORS OF BUSES 7, 11, 14, AND 16 FOR THE RESONANCE MODE

Bus number	PF for the resonance mode ($P_{13} = -0.00674 \pm 16198i$)
Bus-7	0.265142
Bus-11	0.242049
Bus-14	8.31E – 05
Bus-16	1.76E – 05

The kth diagonal element of the sensitivity matrix $S_{\lambda c}$ is called PF of the kth bus, which actually characterizes the combined excitability and observability of the mode at the kth bus. For an unstable or resonance mode, the bus with the largest PF is the main source of the instability and resonance and can be called the most critical bus.

V. 400-MW WIND FARM AS A CASE STUDY

In this paper, a 400-MW wind farm shown in Fig. 2 with aggregated strings is used as a case study to validate the effectiveness of the proposed bus PF analysis. The main electrical grid, transformers, and cables are modeled by Thévenin's equivalent impedance, leakage impedances, and nominal π-model, respectively.

As the system has 16 buses, the dimension of the matrix $\mathbf{G}(p_q)$ is 16×16, which presents the relationships between bus-1 through bus-16. The parameters of the wind farm are presented in Table I. The parameters of grid-side converters (GSCs) are shown in Table II, where they are designed to have acceptable bandwidths. The phase margins are designed to be

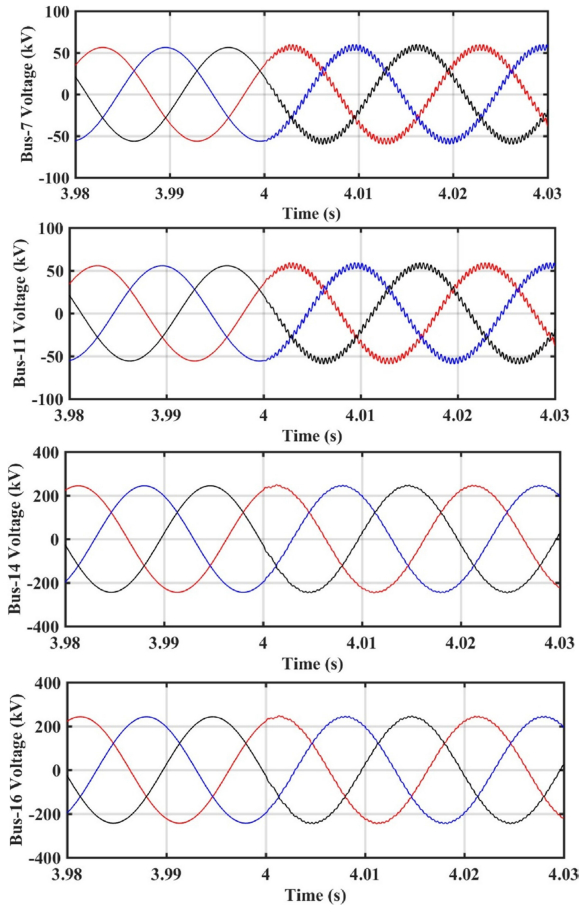

Fig. 7. Voltages of buses 7, 11, 14, and 16, where 3% disturbance is added to the grid voltage at 2578 Hz at $t = 4$ s.

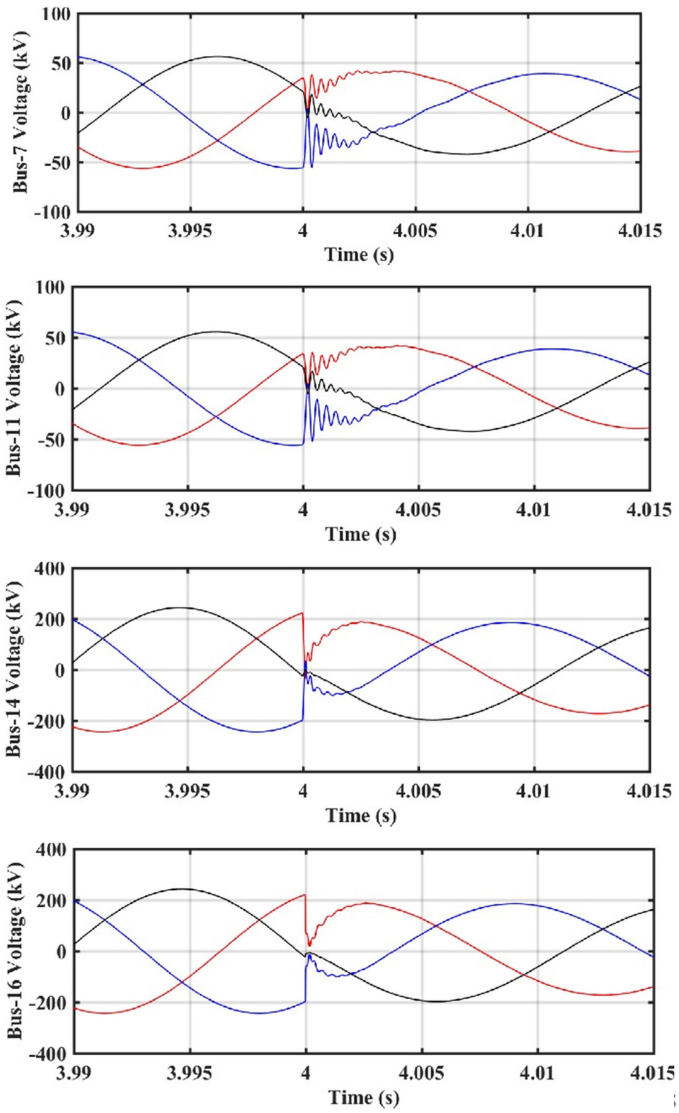

Fig. 8. Voltages of buses 7, 11, 14, and 16, where a voltage sag happens at $t = 4$ s.

around 45° (for a strong grid) to have an acceptable dynamic response. Fig. 3 shows the step response of the GSC-1 under a strong grid, where a good transient repose can be seen. A more detailed explanation about the model can be found in [38].

A. *Proposed Frequency-Domain Analysis and PSCAD Time-Domain Simulations*

In this section, two cases are discussed. For the first case, which is an unstable case, the length of the 150-kV cable is 10 km. For the second case, the cable length is decreased to 5 km to have a stable case but the system still has some modes with very low damping (resonance modes). For both scenarios, the proposed bus PF analysis is applied and corresponding time-domain simulations are performed in the PSCAD/EMTDC environment to validate the analytical analysis.

1) Unstable Case. $L_{cable} = 10$ km (150-kV Cable): In this case, Table III shows the oscillation frequency, the damping, the largest and the smallest PF, and the most and the least influencing bus for the oscillatory modes of the wind farm. The wind farm has one unstable mode, P_9, (critical mode) with the frequency of 839.9 Hz. Therefore, harmonic-frequency oscillations around 840 Hz propagate into the wind farm because of instability problems. Bus-5 has the largest PF, PF = 0.738, for the critical mode, which shows that GSC-4 is the main source of the harmonic instability.

Table IV depicts the PFs of buses 2–5 for the critical mode (P_9). As it can be seen from Table IV, bus-5 (GSC-4) is the most influencing bus on instability, while other buses have not much impact as their PFs are very small.

The wind farm is simulated in PSCAD in the time domain, where the control system is implemented in the s-domain. Therefore, the delay of the SPWM and the digital implementation is modeled by an exponential function ($e^{-1.5T_{s-k}s}$, $T_{s-k} = 0.5/f_{sw}$), as shown in Fig. 1(a) [28]. Fig. 4 shows the currents injected by WT-1, WT-2, WT-3, and WT-4 and Fig. 5 shows their FFT analysis before $t = 4$ s. The total harmonic distortions (THDs) of the currents are different from each other, as the PFs of the buses are different (see Table IV). The THDs of the injected currents of WT-4 and WT-3 are the most and the least, respectively, as bus-5 has the largest PF and bus-4 has the smallest PF in Table IV. The current THD of WT-2 is close to the current THD of WT-3, as their PFs are close together. Therefore, these time-domain simulation results are predicted well by the analytical analysis in Table IV.

In the time-domain simulations shown in Fig. 4, WT-1 is disconnected from the wind farm at $t = 4$ s. Since WT-1 has a very small PF (PF = 0.01), the harmonic-frequency oscillations will remain in the wind farm even after disconnecting WT-1. In Fig. 6, WT-4, the wind turbine with the largest PF (PF = 0.74), is disconnected. Fig. 6 shows that the current oscillations of the other wind turbines will be damped after disconnecting WT-4, which confirms WT-4 is the main source of these oscillations (as predicted in Table IV).

2) Stable Case. $L_{cable} = 5$ km (150-kV Cable): In the second case, the length of the cable is decreased from 10 to 5 km. In this case, the system is stable, i.e., its all modes have negative real parts. However, there are some modes with very small damping, p_{12}, p_{13}, and p_{14}, as presented in Table V. It can be seen that these modes have frequencies around 2.5 kHz and buses 8, 7, and 6 have the largest PFs, where the 33-kV cables are conceded. Therefore, it can be concluded that these modes are most related to the resonances coming from the 33-kV cable.

For example, for the resonance mode p_{13}, with the frequency of 2578 Hz, the PFs of buses 7, 11, 14, and 16 are presented in Table VI. As PFs of buses 7 and 11 are large, these buses are the center of the resonance frequency of 2578 Hz, where the 33-kV cable is connected. On the other hand, buses 14 and 16 have very small PFs. Therefore, buses 7 and 11 give the most disturbance amplification and buses 14 and 16 present the least amplification around the 51st harmonics.

In order to confirm the frequency-domain results predicted by the proposed method in Table VI, the wind farm is simulated using the PSCAD software, where 3% disturbance is added to the grid voltage at 2578 Hz at $t = 4$ s. Fig. 7 shows the voltages

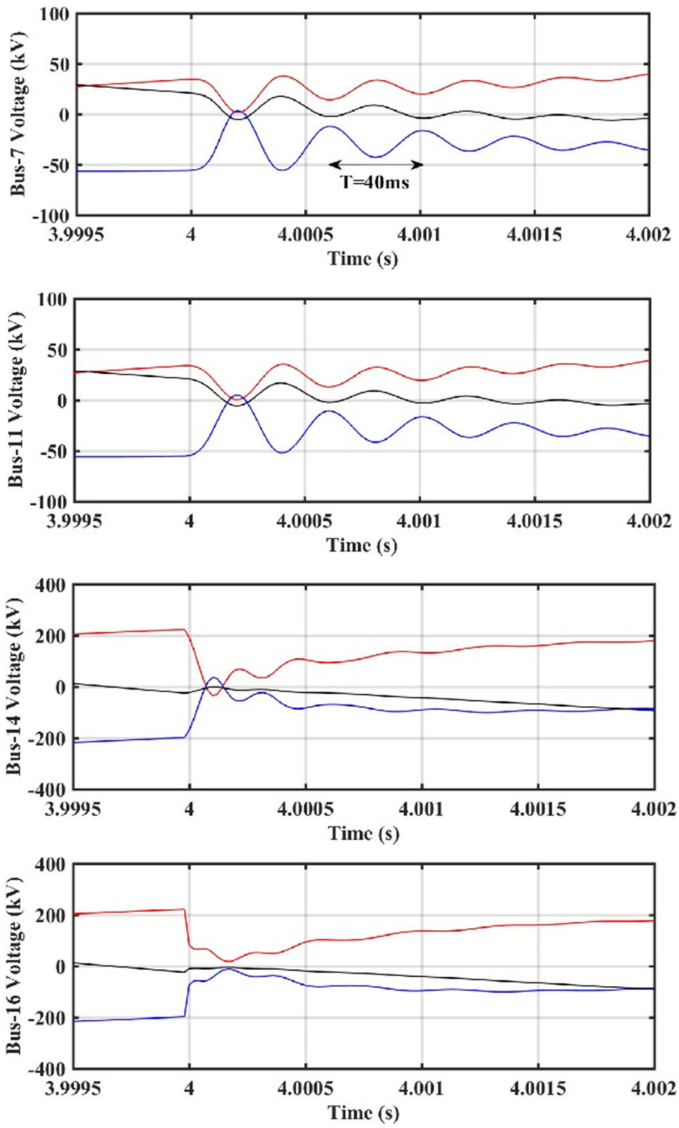

Fig. 9. Zoomed transient waveforms of the voltages shown in Fig. 8 around $t = 4$ s.

of buses 7, 11, 14, and 16. The disturbance amplification of the buses is different from each other, as the PFs of the buses are different in Table VI. The electrical oscillations of bus-7 and bus-16 are the most and the least, respectively, as the frequency-domain results in Table VI predict that bus-7 has the largest PF and bus-16 has the smallest PF. The THD of bus-7 is close to the THD of bus-11, as their PFs are almost the same as well. Therefore, these time-domain simulation results are predicted well by the proposed frequency-domain analysis presented in Table VI.

3) Transient Oscillations: In this test, a fault occurs at $t = 4$ s, which leads to a voltage sag with the depth of 20%. Fig. 8 shows bus voltages 7, 11, 14, and 16, and Fig. 9 shows the zoomed transient waveforms of these voltages around $t = 4$ s. As shown in Fig. 9, the frequencies of the transient oscillations are around 2.5 kHz. In addition, the magnitudes of the oscillations of buses 7 and 11 are much larger than buses 14 and 16. These results are also predicted by the proposed frequency-domain analysis shown in Table VI, where the frequency of the resonance mode p_{13} is 2578 Hz and the PFs of buses 7 and 11 are much larger than buses 14 and 16.

VI. Conclusion

This paper attempts to identify the contribution of each power converter and each bus to harmonic instability in a power electronics based system, and consequently to locate the main source of harmonic instability. A power electronics based system is introduced as a MIMO transfer function matrix and bus PFs are identified by eigenvalue sensitivity analysis versus the elements of the MIMO matrix. A 400-MW wind farm is studied as a power electronics based system for the proposed PF analysis. For unstable conditions, the presented frequency-domain analysis shows that some power converters can have larger PFs than the other converters. Time-domain simulations in PSCAD software confirm that a power electronics based system can go from an unstable operation to a stable operation by disconnecting the power converters with the larger PFs. For stable conditions, the frequency-domain results show that some modes can have very low damping (resonance modes). The presented PF analysis can identify the main bus, which excites these resonance modes, where is the most efficient location for active or passive damping activities. Simulation results confirm that a bus with a larger PF amplifies disturbances (around the frequency of the resonance mode) more than the other buses.

References

[1] B. K. Bose, "Global energy scenario and impact of power electronics in 21st century," *IEEE Trans. Ind. Electron.*, vol. 60, no. 7, pp. 2638–2651, Jul. 2013.

[2] J. M. Carrasco *et al.*, "Power-electronic systems for the grid integration of renewable energy sources: A survey," *IEEE Trans. Ind. Electron.*, vol. 53, no. 4, pp. 1002–1016, Jun. 2006.

[3] F. Blaabjerg, R. Teodorescu, M. Liserre, and A. V. Timbus, "Overview of control and grid synchronization for distributed power generation systems," *IEEE Trans. Ind. Electron.*, vol. 53, no. 5, pp. 1398–1409, Oct. 2006.

[4] F. Jensen, Ł. H. Kocewiak, and Z. Emin, "Amplification of harmonic background distortion in wind power plants with long high voltage connections," presented at the *CIGRE Biennial Session*, Paris, France, Aug. 2016, Paper C4-112.

[5] J. H. R. Enslin and P. J. M. Heskes, "Harmonic interaction between a large number of distributed power inverters and the distribution network," *IEEE Trans. Power Electron.*, vol. 19, no. 6, pp. 1586–1593, Nov. 2004.

[6] T. Messo, J. Jokipii, J. Puukko, and T. Suntio, "Determining the value of dc-link capacitance to ensure stable operation of a three-phase photovoltaic inverter," *IEEE Trans. Power Electron.*, vol. 29, no. 2, pp. 665–673, Feb. 2014.

[7] D. Bazargan, S. Filizadeh, and A. M. Gole, "Stability analysis of converter-connected battery energy storage systems in the grid," *IEEE Trans. Sustain. Energy*, vol. 5, no. 4, pp. 1204–1212, Oct. 2014.

[8] L. Harnefors, M. Bongiorno, and S. Lundberg, "Input-admittance calculation and shaping for controlled voltage-source converters," *IEEE Trans. Ind. Electron.*, vol. 54, no. 6, pp. 3323–3334, Dec. 2007.

[9] M. Cespedes and J. Sun, "Impedance modeling and analysis of grid connected voltage-source converters," *IEEE Trans. Power Electron.*, vol. 29, no. 3, pp. 1254–1261, Mar. 2014.

[10] X. Wang, L. Harnefors, and F. Blaabjerg, "A unified impedance model of grid-connected voltage-source converters," *IEEE Trans. Power Electron.*, vol. 33, no. 2, pp. 1775–1787, Feb. 2014. Doi: 10.1109/TPEL.2017.2684906.

[11] X. Wang, F. Blaabjerg, and W. Wu, "Modelling and analysis of harmonic stability in ac power-electronics-based power system," *IEEE Trans. Power Electron.*, vol. 29, no. 12, pp. 6421–6432, Dec. 2014.

[12] A. Singh, A. K. Kaviani, and B. Mirafzal, "On dynamic models and stability analysis of three-phase phasor PWM-based CSI for stand-alone applications," *IEEE Trans. Ind. Electron.*, vol. 62, no. 5, pp. 2698–2707, May 2015.
[13] E. A. A. Coelho, P. C. Cortizo, and P. F. D. Garcia, "Small-signal stability for parallel-connected inverters in stand-alone ac supply systems," *IEEE Trans. Ind. Appl.*, vol. 38, no. 2, pp. 533–542, Mar. 2002.
[14] N. Pogaku, M. Prodanovic, and T. C. Green, "Modeling, analysis and testing of autonomous operation of an inverter-based microgrid," *IEEE Trans. Power Electron.*, vol. 22, no. 2, pp. 613–625, Mar. 2007.
[15] N. Bottrell, M. Prodanovic, and T. C. Green, "Dynamic stability of a microgrid with an active load," *IEEE Trans. Power Electron.*, vol. 28, no. 11, pp. 5107–5119, Nov. 2013.
[16] F. Gao, X. Zheng, S. Bozhko, C. I. Hill, and G. Asher, "Modal analysis of a PMSG-based DC electrical power system in the more electric aircraft using eigenvalues sensitivity," *IEEE Trans. Transp. Electrif.*, vol. 1, no. 1, pp. 65–76, Jun. 2015.
[17] Z. Shuai, Y. Hu, Y. Peng, C. Tu, and Z. J. Shen, "Dynamic stability analysis of synchronverter-dominated microgrid based on bifurcation theory," *IEEE Trans. Ind. Electron.*, vol. 64, no. 9, pp. 7467–7477, Sep. 2017.
[18] Y. Wang, X. Wang, F. Blaabjerg, and Z. Chen, "Harmonic instability assessment using state-space modeling and participation analysis in inverter-fed power systems," *IEEE Trans. Ind. Electron.*, vol. 64, no. 1, pp. 806–816, Jan. 2017.
[19] L. P. Kunjumuhammed, B. C. Pal, C. Oates, and K. J. Dyke, "Electrical oscillations in wind farm systems: analysis and insight based on detailed modeling," *IEEE Trans. Sustain. Energy*, vol. 7, no. 1, pp. 51–62, Jan. 2016.
[20] Y. Wang, X. Wang, F. Blaabjerg, and Z. Chen, "Small-signal stability analysis of inverter-fed power systems using component connection method," *IEEE Trans. Smart Grid*, early access, 2017.
[21] L. P. Kunjumuhammed, B. C. Pal, C. Oates, and K. J. Dyke, "The adequacy of the present practice in dynamic aggregated modeling of wind farm systems," *IEEE Trans. Sustain. Energy*, vol. 8, no. 1, pp. 23–32, Jan. 2017.
[22] J. Kwon, X. Wang, F. Blaabjerg, C. L. Bak, V. S. Sularea, and C. Busca, "Harmonic interaction analysis in a grid-connected converter using harmonic state-space (HSS) modeling," *IEEE Trans. Power Electron*, vol. 32, no. 9, pp. 6823–6835, Sep. 2017.
[23] E. Ebrahimzadeh, F. Blaabjerg, X. Wang, and C. L. Bak, "Harmonic stability and resonance analysis in large PMSG-based wind power plants," *IEEE Trans. Sustain. Energy*, vol. 9, no. 1, pp. 12–23, Jan. 2018.
[24] A. Rygg and M. Molinas, "Apparent impedance analysis: A small-signal method for stability analysis of power electronic based systems," *IEEE Trans. Emerging Select. Topics Power Electron.*, vol. 5, no. 4, pp. 1474–1486, Dec. 2017. Doi: 10.1109/JESTPE.2017.2729596.
[25] J. Sun, "Impedance-based stability criterion for grid-connected inverters," *IEEE Trans. Power Electron.*, vol. 26, no. 11, pp. 3075–3078, Nov. 2011.
[26] L. Harnefors, R. Finger, X. Wang, H. Bai, and F. Blaabjerg, "VSC input-admittance modeling and analysis above the nyquist frequency for passivity-based stability assessment," *IEEE Trans. Ind. Electron.*, vol. 64, no. 8, pp. 6362–6370, Aug. 2017.
[27] A. Rygg, M. Molinas, C. Zhang, and X. Cai, "A modified sequence-domain impedance definition and its equivalence to the dq-domain impedance definition for the stability analysis of ac power electronic systems," *IEEE Trans. Emerging Sel. Topics Power Electron.*, vol. 4, no. 4, pp. 1383–1396, Dec. 2016.
[28] C. Yoon, H. Bai, R. Beres, X. Wang, C. Bak, and F. Blaabjerg, "Harmonic stability assessment for multi-paralleled, grid-connected inverters," *IEEE Trans. Sustain. Energy*, vol. 7, no. 4, pp. 1388–1397, Oct. 2016.
[29] E. Ebrahimzadeh, F. Blaabjerg, X. Wang, and C. L. Bak, "Modeling and identification of harmonic instability problems in wind farms," in *Proc. IEEE Energy Convers. Congr. Expo.*, Milwaukee, WI, USA, Sep. 2016, pp. 1–6.
[30] E. Ebrahimzadeh, F. Blaabjerg, X. Wang, and C. L. Bak, "Reducing harmonic instability and resonance problems in PMSG based wind farms," *IEEE Trans. Emerging Sel. Topics Power Electron.*, vol. 6, no. 1, pp. 73–83, Mar. 2018.
[31] J. Wang, J. D. Yan, L. Jiang, and J. Zou, "Delay-dependent stability of single-loop controlled grid-connected inverters with LCL filters," *IEEE Trans. Power Electron.*, vol. 31, no. 1, pp. 743–757, Jan. 2016.
[32] X. Li, X. Wu, Y. Geng, X. Yuan, C. Xia, and X. Zhang, "Wide damping region for LCL-type grid-connected inverter with an improved capacitor current-feedback method," *IEEE Trans. Power Electron.*, vol. 30, no. 9, pp. 5247–5259, Sep. 2015.
[33] C. Chen, J. Xiong, Z. Wan, J. Lei, and K. Zhang, "A Time delay compensation method based on area equivalence for active damping of an LCL-type converter," *IEEE Trans. Power Electron.*, vol. 32, no. 1, pp. 762–772, Jan. 2017.
[34] S. Skogestad and I. Postlethwaite, *Multivariable Feedback Control: Analysis and Design*. New York, NY, USA: Wiley, 2000.
[35] Y. Cui and X. Wang, "Modal frequency sensitivity for power system harmonic resonance analysis," *IEEE Trans. Power Deliv.*, vol. 27, no. 2, pp. 1010–1017, Apr. 2012.
[36] E. Ebrahimzadeh, F. Blaabjerg, X. Wang, and C. L. Bak, "Dynamic resonance sensitivity analysis in wind farms," in *Proc. IEEE 8th Int. Symp. Power Electron. Distrib. Gener. Syst.*, Florianopolis, Brazil, 2017, pp. 1–5.
[37] K. N. B. M. Hasan, K. Rauma, A. Luna, J. I. Candela, and P. Rodriguez, "Harmonic compensation analysis in offshore wind power plants using hybrid filters," *IEEE Trans. Ind. Appl.*, vol. 50, no. 3, pp. 2050–2060, May/Jun. 2014.
[38] S. K. Chaudhary, "Control and protection of wind power plants with VSC-HVDC connection," Ph.D. dissertation, Aalborg Univ., Aalborg, Denmark, 2011.

Esmaeil Ebrahimzadeh (S'16) received the M.Sc. degree in electrical engineering from the University of Tehran, Tehran, Iran, in 2013. Since 2015, he has been working toward the Ph.D. degree at the Department of Energy Technology, Aalborg University, Aalborg, Denmark.

He has been a Lecturer for undergraduate Lab courses with the University of Tehran. He was a Visiting R&D Engineer with Vestas Wind Systems A/S, Aarhus, Denmark, in 2017. His research interests include modeling, design, and control of power-electronic converters in different applications like renewable energy systems, and his main current project is focusing on power quality and stability analysis in large wind power plants.

Mr. Ebrahimzadeh was a recipient of the best paper awards at IEEE PEDG 2016 and IEEE PES GM 2017.

Frede Blaabjerg (S'86–M'88–SM'97–F'03) received the Ph.D. degree from Aalborg University, Aalborg, Denmark, in 1992.

He was with ABB-Scandia, Randers, Denmark, from 1987 to 1988. He became an Assistant Professor in 1992, an Associate Professor in 1996, and a Full Professor of power electronics and drives in 1998. From 2017, he became a Villum Investigator. He has authored or coauthored more than 450 journal papers in the fields of power electronics and its applications. He is the Co-Author of two monographs and the Editor of six books in power electronics and its applications. His current research interests include power electronics and its applications such as in wind turbines, photovoltaic systems, reliability, harmonics, and adjustable speed drives.

Dr. Blaabjerg was a recipient of 22 IEEE Prize Paper Awards, the IEEE PELS Distinguished Service Award in 2009, the EPE-PEMC Council Award in 2010, the IEEE William E. Newell Power Electronics Award 2014, and the Villum Kann Rasmussen Research Award 2014. He was the Editor-in-Chief of the IEEE TRANSACTIONS ON POWER ELECTRONICS from 2006 to 2012. He has been a Distinguished Lecturer for the IEEE Power Electronics Society from 2005 to 2007 and for the IEEE Industry Applications Society from 2010 to 2011 as well as 2017 to 2018. He was nominated from 2014 to 2017 by Thomson Reuters to be among the most 250 cited researchers in Engineering in the world. In 2017, he became the Honoris Causa at the University Politehnica Timisoara, Timisoara, Romania.

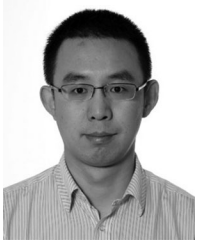

Xiongfei Wang (S'10–M'13–SM'17) received the B.S. degree in electrical engineering from Yanshan University, Qinhuangdao, China, in 2006, the M.S. degree in electrical engineering from the Harbin Institute of Technology, Harbin, China, in 2008, and the Ph.D. degree in energy technology from Aalborg University, Aalborg, Denmark, in 2013.

Since 2009, he has been with Aalborg University, Aalborg, Denmark, where he is currently an Associate Professor with the Department of Energy Technology. His research interests include modeling and control of grid-connected converters, harmonics analysis and control, passive and active filters, and stability of power electronic based power systems.

Dr. Wang serves as an Associate Editor for the IEEE TRANSACTIONS ON POWER ELECTRONICS, the IEEE TRANSACTIONS ON INDUSTRY APPLICATIONS, and the IEEE JOURNAL OF EMERGING AND SELECTED TOPICS IN POWER ELECTRONICS. He was a recipient of the second prize paper award and the outstanding reviewer award of the IEEE TRANSACTIONS ON POWER ELECTRONICS in 2014 and 2016, respectively, and the best paper awards at IEEE PEDG 2016 and IEEE PES GM 2017.

Claus Leth Bak (M'99–SM'07) was born in Århus, Denmark, in April 13, 1965. He received the B.Sc. (with honors) and M.Sc. degrees in electrical power engineering from the Department of Energy Technology (ET), Aalborg University (AAU), Aalborg, Denmark, in 1992 and 1994, respectively, and the Ph.D. degree in electrical power engineering with the thesis "EHV/HV underground cables in the transmission system" from Aalborg University, in 2015.

After his studies, he worked as a Professional Engineer with the Electric Power Transmission and Substations with specializations within the area of power system protection with the NV Net Transmission Company. In 1999, he was an Assistant Professor with ET-AAU, where he holds a Full Professor position currently. He serves as the Head of the Energy Technology Ph.D. program (more than 100 Ph.D. degrees) and as the Head of the Section of Electric Power Systems and High Voltage in AAU and is a Member of the Ph.D. board with the Faculty of Engineering and Science. He has supervised/co-supervised $+35$ Ph.D. degrees and $+50$ M.Sc. theses. He is the Author/Co-Author of approximately 240 publications. His main research interests include corona phenomena on overhead lines, power system modeling and transient simulations, underground cable transmission, power system harmonics, power system protection, and HVDC voltage-source converter offshore transmission networks.

Dr. Bak was a recipient of the DPSP 2014 best paper award and the PEDG 2016 best paper award. He is a Member of Cigré JWG C4-B4.38, Cigré SC C4 and SC B5 study committees' member, and Danish Cigré National Committee.